OUTLOOK
The future of medicine

nature

THE INTERNATIONAL WEEKLY JOURNAL OF SCIENCE

JUPITER REVISITED

Juno mission offers a fresh perspective on the gas giant **PAGES 168, 216, 220, 223 & 227**

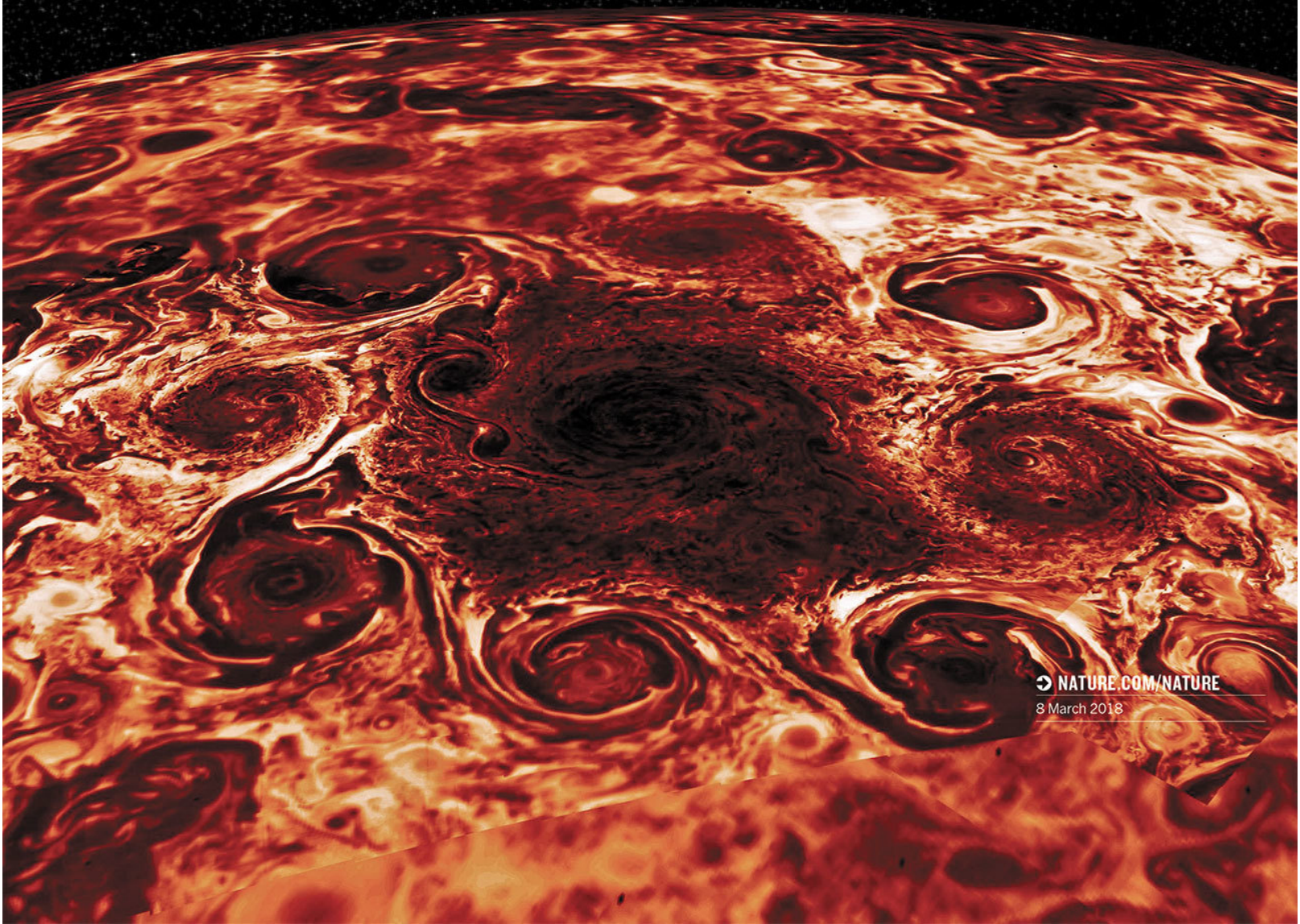

NATURE.COM/NATURE
8 March 2018

LETTER

doi:10.1038/nature25491

Clusters of cyclones encircling Jupiter's poles

A. Adriani[1], A. Mura[1], G. Orton[2], C. Hansen[3], F. Altieri[1], M. L. Moriconi[4], J. Rogers[5], G. Eichstädt[6], T. Momary[2], A. P. Ingersoll[7], G. Filacchione[1], G. Sindoni[1], F. Tabataba-Vakili[2], B. M. Dinelli[4], F. Fabiano[4,8], S. J. Bolton[9], J. E. P. Connerney[10], S. K. Atreya[11], J. I. Lunine[12], F. Tosi[1], A. Migliorini[1], D. Grassi[1], G. Piccioni[1], R. Noschese[1], A. Cicchetti[1], C. Plainaki[13], A. Olivieri[13], M. E. O'Neill[14], D. Turrini[1,15], S. Stefani[1], R. Sordini[1] & M. Amoroso[13]

The familiar axisymmetric zones and belts that characterize Jupiter's weather system at lower latitudes give way to pervasive cyclonic activity at higher latitudes[1]. Two-dimensional turbulence in combination with the Coriolis β-effect (that is, the large meridionally varying Coriolis force on the giant planets of the Solar System) produces alternating zonal flows[2]. The zonal flows weaken with rising latitude so that a transition between equatorial jets and polar turbulence on Jupiter can occur[3,4]. Simulations with shallow-water models of giant planets support this transition by producing both alternating flows near the equator and circumpolar cyclones near the poles[5–9]. Jovian polar regions are not visible from Earth owing to Jupiter's low axial tilt, and were poorly characterized by previous missions because the trajectories of these missions did not venture far from Jupiter's equatorial plane. Here we report that visible and infrared images obtained from above each pole by the Juno spacecraft during its first five orbits reveal persistent polygonal patterns of large cyclones. In the north, eight circumpolar cyclones are observed about a single polar cyclone; in the south, one polar cyclone is encircled by five circumpolar cyclones. Cyclonic circulation is established via time-lapse imagery obtained over intervals ranging from 20 minutes to 4 hours. Although migration of cyclones towards the pole might be expected as a consequence of the Coriolis β-effect, by which cyclonic vortices naturally drift towards the rotational pole, the configuration of the cyclones is without precedent on other planets (including Saturn's polar hexagonal features). The manner in which the cyclones persist without merging and the process by which they evolve to their current configuration are unknown.

NASA's Juno spacecraft[10,11] has been operating in a 53-day highly elliptical polar orbit of Jupiter since 5 July 2016. The spacecraft has passed close to Jupiter six times now, on five of which occasions instruments on board were able to sound the planet and observe many interesting atmospheric structures[12–15]. The Juno spacecraft is in a high-inclination orbit with perijove (the point in its orbit nearest Jupiter's centre) approximately 4,000 km above the cloud tops, passing from pole to equator to pole in about two hours. From their unique vantage point above the poles, JIRAM[16,17] (Jupiter InfraRed Auroral Mapper) and JunoCam[18], onboard Juno, obtained unprecedented views of Jupiter's polar regions. JIRAM is an infrared imager suitable for atmospheric mapping and JunoCam is a pushframe visible camera. Jupiter fly-bys took place during perijove passes PJ1 on 28 August 2016, PJ3 on 11 December 2016, PJ4 on 2 February 2017 and PJ5 on 27 March 2017 (no remote-sensing observations were collected during PJ2).

The atmospheric structure in Jupiter's polar regions is very different from the well known axisymmetric banding of alternating belts and zones at lower latitudes. The polar turbulence predicted by models is consistent with initial close-up observations in the visible part of the spectrum[15]. Cyclones, as opposed to anticyclones, were expected in the polar regions as a result of the Coriolis β-effect[9,19,20]. What was unexpected is their stable appearance, close clustering and symmetry around each of the poles.

The Northern Polar Cyclone (NPC, Fig. 1) has a diameter of approximately 4,000 km (on the JIRAM infrared images). It is offset relative to the geographic north pole of Jupiter by about 0.5° and is surrounded by eight circumpolar cyclones (henceforth referred to as just 'cyclones') in a double-squared geometric pattern (Figs 1 and 2). Counting alternating cyclones, four are centred at about 83.3° N and the other four are centred at about 82.5° N. The square formed by the latter four cyclones is shifted with respect to the square formed by the former four cyclones by 45° longitude, forming a 'ditetragonal' shape, in which the angular distances between the centre of one cyclone and the next vary from 43° to 47°. All cyclones have similar dimensions with diameters ranging from 4,000 km to 4,600 km. Spiral arms are prominent in their outer regions, but tend to disappear in their inner regions except in the NPC itself. These arms define an additional sphere of influence beyond the cores of the cyclones in which co-rotating material can be found. The four cyclones furthest from the NPC have broad cloud-covered inner regions with sharp oblate boundaries. The four cyclones interspersed between them have more diverse and irregular inner regions, with very small-scale cloud textures; some of them appear chaotic and turbulent.

The Southern Polar Cyclone (SPC, Figs 1 and 2) is surrounded by five large circumpolar cyclones in a quasi-pentagonal pattern. They are of similar size, but are generally bigger than the northern cyclones, with diameters ranging between 5,600 km and 7,000 km. The southern cyclones present a range of morphologies, although the differences are much less distinct than in the north. In particular, some of them display a quasi-laminar circulation: the SPC and two adjacent cyclones have cloud spirals converging to the centre, while the other three cyclones appear to be very turbulent along their spiral cloud branches. The SPC has an offset of about 1°–2° relative to the geographic south pole and the angular distance between two adjacent cyclones is not as regular as in the north: it can vary from 65° to 80° relative to the centre of rotation of the SPC.

Figures 1 and 2 show the correspondence between the features in JIRAM maps and in JunoCam images. Regions that are relatively bright in the JunoCam images are cool in the JIRAM thermal infrared images and regions that are relatively dark in the visible are warm. Because the JIRAM thermal radiance in the approximately 5-μm M-band is primarily governed by cloud opacity, regions that appear warm can be interpreted as relatively clear of clouds, allowing radiance from deeper, warmer regions to be detected, and regions that appear cold must be cloudier.

[1]INAF-Istituto di Astrofisica e Planetologia Spaziali, Roma, Italy. [2]Jet Propulsion Laboratory, California Institute of Technology, Pasadena, California, USA. [3]Planetary Science Institute, Tucson, Arizona, USA. [4]CNR-Istituto di Scienze dell'Atmosfera e del Clima, Bologna e Roma, Italy. [5]British Astronomical Association, Burlington House, Piccadilly, London W1J 0DU, UK. [6]Alexanderstraße 21, 70184 Stuttgart, Germany. [7]Division of Geology and Planetary Sciences, California Institute of Technology, Pasadena, California, USA. [8]Dipartimento di Fisica e Astronomia, Università di Bologna, Bologna, Italy. [9]Space Science and Engineering Division, Southwest Research Institute, San Antonio, Texas, USA. [10]Code 695, NASA/Goddard Space Flight Center, Greenbelt, Maryland, USA. [11]Planetary Sciences Laboratory, University of Michigan, Ann Arbor, Michigan, USA. [12]Center for Astrophysics and Space Science, Cornell University, Ithaca, New York, USA. [13]Agenzia Spaziale Italiana, Roma, Italy. [14]Department of the Geophysical Sciences, University of Chicago, Chicago, Illinois, USA. [15]Departamento de Fisica, Universidad de Atacama, Copayapu 485, Copiapò, Chile.

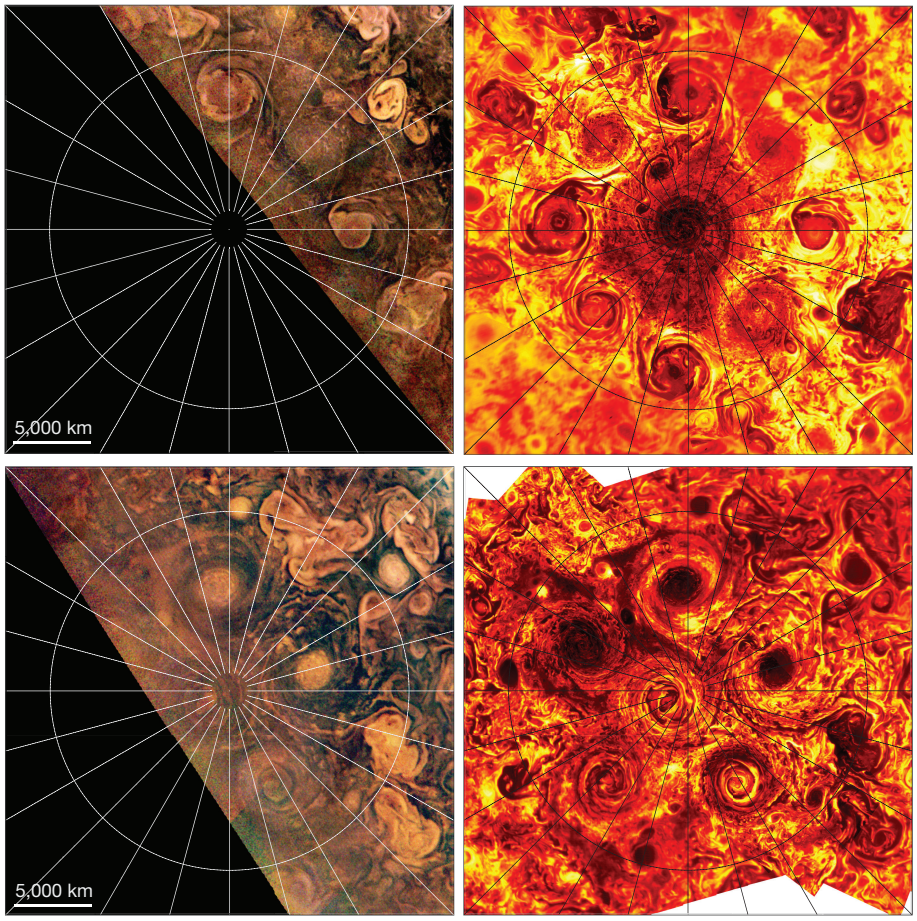

Figure 1 | The poles of Jupiter as they appear at visible and infrared wavelengths. Projected maps of the regions surrounding the north pole (top) and south pole (bottom) from the JIRAM 5-μm M-filter observations (right panels) and JunoCam colour-composite images (left panels) during PJ4 on 2 February 2017. The latitude circle is 80° N or 80° S (planetocentric). Meridians are drawn every 15° of longitude, and 0° W in System III is positioned at the centre right of the images. By operating at thermal-infrared wavelengths, JIRAM observes the atmospheric structures regardless of solar illumination, whereas JunoCam's optical images are restricted to only the illuminated hemisphere, which is why only part of the JunoCam map for the north pole is present. JIRAM radiance, ranging from 0.02 W m^{-2} sr^{-1} (dark red) to 0.8 W m^{-2} sr^{-1} (white) is corrected with respect to the emission angle; the radiance scale is logarithmic. The JunoCam images are corrected with respect to solar illumination angle, as discussed in ref. 5 and the colours of the maps have been stretched and balanced to enhance atmospheric features. Cyclonic features can be seen clustered around each pole with regular circular shapes, some with spiral arms. For the south polar region, we note that there is a wider longitude separation (a 'gap') between the cyclones near 180° W (centre left side) than between the other cyclones. Two smaller cold (dark red) features can be seen to the upper left of the NPC, which are anticyclonic vortices.

Thus, the visibly bright discrete features in the JunoCam images in Figs 1 and 2 correspond to high-altitude clouds, while the darker background corresponds to a deeper cloud deck. This corresponds to a general qualitative result from JunoCam observations made during PJ1, that visually bright regions correspond to regions that are also relatively bright in the 890-nm band, which is sensitive to absorption by methane gas, implying high-altitude clouds in those regions[14]. Figure 3, with the highest-resolution maps of the polar regions, gives a detailed view of the polar morphologies, showing JIRAM images corresponding to brightness temperatures in the range 190–260 K.

In most cases, the cyclones are essentially in contact if the spiral arms that extend beyond the core are included. In some cases, a single

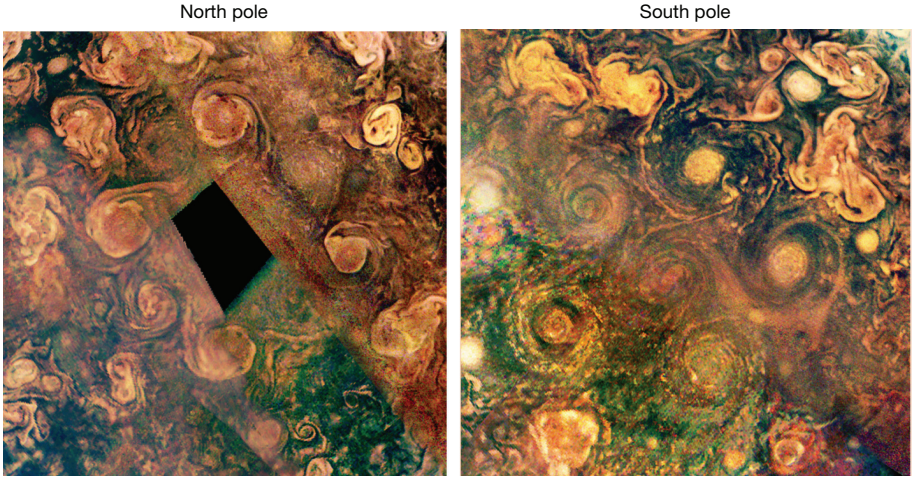

Figure 2 | The poles observed by JunoCam during the first four passes at Jupiter. A composite is shown of the polar regions observed by JunoCam not only during PJ4 but also at complementary longitudes, acquired during PJ1, PJ3 and PJ5 for regions not illuminated by sunlight during PJ4. The PJ4 projection has been preserved as in the left panels in Fig. 1; the remainder of the unfilled space is covered by a composite of images from the other perijove passes. The remaining regions that are dark in the left panels of Fig. 1 are a smooth composite of JunoCam images taken during PJ1, PJ3 and PJ5. The area in the centre of the north polar region (left panel) is dark because those latitudes were not illuminated. Elsewhere on Jupiter, cyclonic circulations assume various forms, especially at high latitudes, but none is a simple spiral with a circular outline, except for some very small ones. We note that, although they were imaged 53–106 days (1–2 Juno orbits) from the PJ4 observations, the positions and even the gross morphologies of the cyclones imaged during those orbits are not very different from their overall morphology in the PJ4 JIRAM map. The JunoCam map colours were chosen to enhance atmospheric features.

Table 1 | Spin velocities of the single cyclones

North pole				South pole			
Circumpolar cyclone number	Angular velocity (deg min^{-1})	Tangent velocity (km h^{-1})	Full rotation hours	Circumpolar cyclone number	Angular velocity (deg min^{-1})	Tangent velocity (km h^{-1})	Full rotation hours
NPC	0.17	267	35.3	SPC	0.19	299	31.6
1	0.22	343	27.5	1 (H)	0.13	204	46.1
3 (D)	0.21	337	28.0	2	0.17	273	34.5
4 (E)	0.10	157	60.0	3	0.16	252	37.5
5 (F)	0.12	296	48.0	4	0.21	330	28.6
6	0.19	295	32.0	5 (G)	0.17	273	34.5
7	0.22	354	26.6				
8	0.12	296	48.0				

Spin velocities were calculated at the radial distance of approximately 1,500 km from the spinning centres during PJ4 by JIRAM images. There were not enough data to compute the velocity of northern circumpolar cyclone 2. The numbering of the northern circumpolar cyclones goes from 1 to 8 proceeding anticlockwise, with circumpolar cyclone 1 the one located at 0° longitude. The numbering of the southern circumpolar cyclones starts from the circumpolar cyclone at 150° longitude and proceeds anticlockwise. Letters in parentheses identify the circumpolar cyclone, if present, in Extended Data Fig. 1. A quick calculation assuming the gradient wind balance, which includes Coriolis, centrifugal and pressure forces, indicates pressure gradients of about 5–10 Pa km^{-1} at 1,500 km from the circumpolar cyclone centres.

cloud streak connects the outer spiral arms of adjacent cyclones and can be seen to be continuously stretched. The SPC is in contact with the five cyclones around it. By contrast, the PJ4 JIRAM animation (see Supplementary Videos) reveals a chaotic zone between the NPC and the eight surrounding cyclones, within which there is a largely continuous westward (clockwise) flow at about 86° N; poleward of this, the eastward (anticlockwise) flow of the NPC begins. This chaotic zone appears to contain turbulent small-scale cloud textures and a few small anticyclonic vortices. The largest of these, located between the NPC and the cyclones, may be identical to a similar anticyclonic vortex at PJ5, having moved westward by 31° longitude in Juno's 53-day orbital period. JIRAM data acquired during PJ4 cover a time span of about 2 h at each pole, enabling us to monitor the movements of the clouds and other structures that are evident within each cyclone, which in turn permits the identification of cyclonic and anticyclonic zones. The velocity field inside each cyclone is not straightforward to evaluate from these data, both because the pointing inaccuracy of JIRAM is not negligible when dealing with fine-scale structures inside cyclones, and because detailed structures whose movement is visible are not scattered uniformly. Table 1 provides a summary of preliminary JIRAM measurements of the rotational speeds of individual cyclones at 1,500 km from their respective centres.

The changes occurring in the polar polygons can be seen by the JIRAM observations with a time lapse of about 53 terrestrial days between PJ4 and PJ5 (Extended Data Fig. 1). By this analysis, the northern eight cyclones appear to drift very slowly around the north pole (or around the NPC), by approximately 2.6° eastward in System III longitude. The changes between the observations taken by JunoCam are based on images of the sunlit side of the poles during PJ1, PJ3, PJ4 and PJ5. On the other hand, JunoCam polar images have an overlap of about 90°–180° in sunlit longitudes between successive perijove observations in similar 53-day intervals, and can also be compared with the complete map from JIRAM at PJ4. They show that the eight cyclones are preserved throughout the entire seven-month period, retaining their individual morphological characteristics, and showing only minor movements (Fig. 2). The visible sector of the octagon rotated around the north pole as follows (positive is westward): PJ1 to PJ3, about +2°; PJ3 to PJ4, −4° to −7.5°; PJ4 to PJ5, 0° to −3.5°. Thus the octagon has not shown any progressive rotation about the pole in System III longitudes. Both instruments observe small meridional displacements

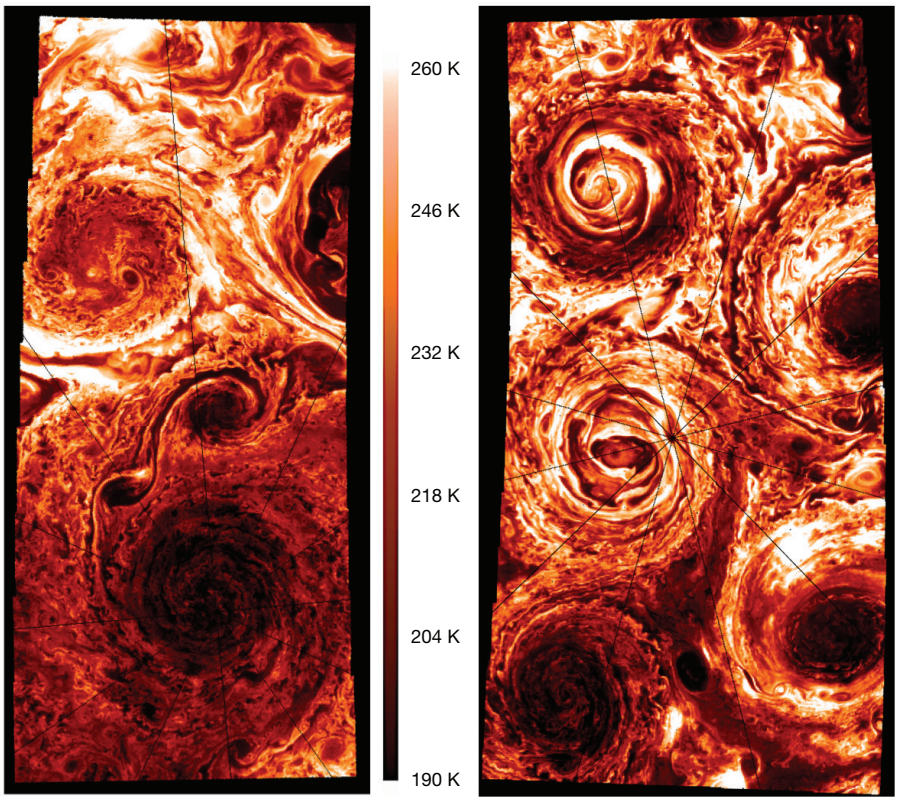

Figure 3 | High-resolution view of the polar vortices. The left panel shows the north pole as seen in the 5-μm spectral region (JIRAM M-filter) at an average spatial resolution of 18 km per pixel. The right panel shows the south pole at an average spatial resolution of 25 km per pixel in the same filter. These maps represent the highest available spatial resolution of JIRAM images during PJ4. The red colour scale from black to white is associated with the apparent brightness temperature shown, covering 190–260 K. Some cyclones look more clearly structured with alternating cold (cloudier) and warm (clearer) banding as a function of radius. It also clearly depicts the mesoscale dynamics over Jupiter's polar regions, showing a chaotic environment with many wavy structures and smaller anticyclones and cyclones developing among the largest ones. Such small anticyclonic eddies can be seen between some of the cyclones, especially around the NPC, where the largest of them measures about 1,200 km in diameter. There is a great structural difference between the NPC, which is dominated by a very small-scale cloud structure, and the SPC, which is characterized by a quasi-laminar behaviour. The SPC has a diameter of about 5,800 km and its centre is very peculiar, presenting an elongated 'eye' shape instead of the circular structure characterizing the centre of all of the other cyclones.

of individual cyclones of the same order of magnitude. For the cyclones at the south pole, JunoCam comparisons between perijove passes do suggest a progressive anticlockwise zonal rotation relative to the SPC of +1° every 53 days, as well as some wandering of individual cyclones. There are large variations in the spacing of the cyclones around the pentagon, associated with the opening and closing of a gap that is always present between two of the cyclones. Just as in the north, the cyclones have preserved their individual morphologies over the seven months of observations.

Two questions arise from these data. The first is why the pentagon and octagon drift so slowly or not at all. By Stokes' theorem, net cyclonic vorticity at the centre would imply cyclonic circulation around the periphery. The other question is why the vortices do not merge. Saturn has a single cyclonic vortex at each pole. By analysing the conditions for formation of each Saturn vortex and comparing them with the conditions on Jupiter, it was predicted that the polar circulation could be different on Jupiter[9]. Some studies[21], applying the theory to the merger of Jupiter's white ovals in 1998–2000, have also shown that like-signed vortices merge on a fast, advective timescale of four months when they are no longer separated by opposite-signed vortices in a single path, a 'vortex street'. Mergers of the polar cyclones are possible, but they have not occurred over seven months of observation, nor is there any evidence of new structures appearing inside the cyclone polygons. Finally, on the other hand, other studies[22,23] show that polygonal vortex patterns (vortex crystals) can develop owing to interaction with a background of weaker vorticity and last indefinitely in a two-dimensional Euler flow.

Online Content Methods, along with any additional Extended Data display items and Source Data, are available in the online version of the paper; references unique to these sections appear only in the online paper.

Received 24 July; accepted 15 November 2017.

1. Porco, C. C. *et al.* Cassini imaging of Jupiter's atmosphere, satellites, and rings. *Science* **299,** 1541–1547 (2003).
2. Rhines, P. B. Waves and turbulence on a beta-plane. *J. Fluid Mech.* **69,** 417–443 (1975).
3. Theiss, J. Equatorward energy cascade, critical latitude, and the predominance of cyclonic vortices in geostrophic turbulence. *J. Phys. Oceanogr.* **34,** 1663–1678 (2004).
4. Sayanagi, K. M., Showman, A. P. & Dowling, T. E. The emergence of multiple robust zonal jets from freely evolving, three-dimensional stratified geostrophic turbulence with applications to Jupiter. *J. Atmos. Sci.* **65,** 3947–3962 (2008).
5. Cho, J. Y. K. & Polvani, L. M. The emergence of jets and vortices in freely evolving, shallow-water turbulence on a sphere. *Phys. Fluids* **8,** 1531–1552 (1996).
6. Iacono, R., Struglia, M. V. & Ronchi, C. Spontaneous formation of equatorial jets in freely decaying shallow water turbulence. *Phys. Fluids* **11,** 1272–1274 (1999).
7. Showman, A. P. Numerical simulations of forced shallow-water turbulence: effects of moist convection on the large-scale circulation of Jupiter and Saturn. *J. Atmos. Sci.* **64,** 3132–3157 (2007).
8. Scott, R. K. & Polvani, L. M. Forced-dissipative shallow-water turbulence on the sphere and the atmospheric circulation of the giant planets. *J. Atmos. Sci.* **64,** 3158–3176 (2007).
9. O'Neill, M. E., Emanuel, K. A. & Flierl, G. R. Polar vortex formation in giant-planet atmospheres due to most convection. *Nat. Geosci.* **8,** 523–526 (2015).
10. Bolton, S. J. *et al.* Jupiter's interior and deep atmosphere: the initial pole-to-pole passes with the Juno spacecraft. *Science* **356,** 821–825 (2017).
11. Connerney, J. E. P. *et al.* Jupiter's magnetosphere and aurorae observed by the Juno spacecraft during its first polar orbits. *Science* **356,** 826–832 (2017).
12. Grassi, D. *et al.* Preliminary results on the composition of Jupiter's troposphere in hot spot regions from the JIRAM/Juno instrument. *Geophys. Res. Lett.* **44,** 4615–4624 (2017).
13. Sindoni, G. *et al.* Characterization of the white ovals on Jupiter's southern hemisphere using the first data by the Juno/JIRAM instrument. *Geophys. Res. Lett.* **44,** 4660–4668 (2017).
14. Orton, G. S. *et al.* The first close-up images of Jupiter's polar regions: results from the Juno mission JunoCam instrument. *Geophys. Res. Lett.* **44,** 4599–4606 (2017).
15. Orton, G. S. *et al.* Multiple-wavelength sensing of Jupiter during the Juno mission's first perijove passage. *Geophys. Res. Lett.* **44,** 4607–4614 (2017).
16. Adriani, A. *et al.* JIRAM, the Jovian Infrared Auroral Mapper. *Space Sci. Rev.* **213,** 393–446 (2017).
17. Adriani, A. *et al.* Juno's Earth flyby: the Jovian Infrared Auroral Mapper preliminary results. *Astrophys. Space Sci.* **361,** 272 (2016).
18. Hansen, C. J. *et al.* JunoCam: Juno's Outreach Camera. *Space Sci. Rev.* **213,** 475–506 (2017).
19. Theiss, J. A generalized Rhines effect and storms on Jupiter. *Geophys. Res. Lett.* **33,** L08809 (2006).
20. LeBeau, R. P. Jr & Dowling, T. E. EPIC simulations of time-dependent, three-dimensional vortices with application to Neptune's great dark spot. *Icarus* **132,** 239–265 (1998).
21. Youssef, A. & Marcus, P. S. The dynamics of jovian white ovals from formation to merger. *Icarus* **162,** 74–93 (2003).
22. Fine, K. S., Cass, A. C., Flynn, W. G. & Driscoll, C. F. Relaxation of 2D turbulence to vortex crystals. *Phys. Res. Lett.* **75,** 3277–3280 (1995).
23. Schecter, D. A., Dubin, D. H. E., Fine, K. S. & Driscoll, C. F. Vortex crystals from 2D Euler flow: experiment and simulation. *Phys. Fluids* **11,** 905–914 (1999).

Supplementary Information is available in the online version of the paper.

Acknowledgements The JIRAM project is founded by the Italian Space Agency (ASI). In particular this work has been developed under the ASI-INAF agreement number 2016-23-H.0. The JunoCam instrument and its operations are funded by the National Aeronautics and Space Administration. A portion of this work was supported by NASA funds to the Jet Propulsion Laboratory, to the California Institute of Technology, and to the Southwest Research Institute. A.P.I. was supported by NASA funds to the Juno project and by NSF grant number 1411952.

Author Contributions A.A. and C.H. are the Juno mission instrument leads for the JIRAM and JunoCam instruments, respectively, and they planned and implemented the observations discussed in this paper. S.J.B. and J.E.P.C. are respectively the principal and the deputy responsible for the Juno mission. A.A., A. Mura, G.O., J.R., A.I. and F.T.-V. were responsible for writing substantial parts of the paper. M.E.O'N. helped with the interpretation of the cyclonic structure. A. Mura, F.A., M.L.M. and D.G. were responsible for reduction and measurement of the JIRAM data and their rendering into graphical formats. G.E., T.M., G.O. and J.R. were responsible for the same tasks for JunoCam data. F.T.-V. and F.F. were responsible for the geometric calibration of the JIRAM data. G.F., G.S., B.M.D. and S.S. were responsible for the JIRAM data radiance calibrations. A.C., R.N. and R.S. were responsible for the JIRAM ground segment. S.K.A., J.I.L., A. Migliorini, D.T, G.P. and D.T. supervised the work. C.P., A.O. and M.A. were responsible for the JIRAM project from the Italian Space Agency side.

Author Information Reprints and permissions information is available at www.nature.com/reprints. The authors declare no competing financial interests. Readers are welcome to comment on the online version of the paper. Publisher's note: Springer Nature remains neutral with regard to jurisdictional claims in published maps and institutional affiliations. Correspondence and requests for materials should be addressed to A.A. (alberto.adriani@iaps.inaf.it).

METHODS

The Jovian InfraRed Auroral Mapper. The Jovian InfraRed Auroral Mapper (JIRAM) is composed of an imager and a spectrometer that share the same telescope[16,17]. The imager focal plane is equipped to observe the planet through a bandpass filter centred at 4.78 μm with a 480-nm bandwidth (M-band) and a bandpass filter centred at 3.45 μm with a 290-nm bandwidth (L-band). The spectrometer's slit is optically co-located with the imager's field of view and its spectral range covers the 2–5-μm interval in 336 spectral bins (bands) resulting in a spectral sampling of 8.9 nm per band across the full spectral range. The instrument design allows for acquisition of simultaneous imager and spectrometer observations: in this study, we used the data from the M-band filter, which covers a field of view of about 1.75° by 6° with 128 × 432 pixels. The instantaneous field of view is 240 μrad (see ref. 16 for instrumental details).

At the time of the observations, the Juno spacecraft was spinning almost perpendicular to the orbital plane. For each spin, JIRAM takes two images: one to the target (nadir direction), and one to the anti-nadir direction, to evaluate the background, which is removed onboard. JIRAM is also equipped with a de-spinning mirror that compensates for the spacecraft rotation and enables it to keep the target image in the field of view during the data acquisition. The de-spinning mirror may also be activated at different times with respect to the nadir direction, allowing a scan of the planet in the spacecraft's spinning plane. No pointing outside the spinning plane is permitted.

The data shown in this paper (integrated radiance from 4.5 μm to 5 μm) have been taken with 12 ms of integration time, resulting in a noise-equivalent radiance lower than 5×10^{-5} W sr^{-1} m^{-2}. Table 1 shows exact times of observations (start time, stop time and number of observations in that sequence or scan). JIRAM observed both poles with high image quality and spatial resolution during PJ4 and PJ5. Polar coverage during PJ4 was complete for regions within 30° latitude of both poles with a spatial resolution varying between 12 km per pixel and 96 km per pixel for the north pole and between 21 km per pixel and 62 km per pixel for the south pole. JIRAM coverage of the poles during PJ5 was incomplete, limited by JIRAM's field of view and Juno's spin axis orientation at perijove.

For PJ4 at the north pole we have complete data coverage with good emission angle (that is, close to 90°), but to cover other parts of the planet we also use radiance emitted at lower angles. Such radiance is partially depleted because the absorption due to cold clouds occurs over a longer atmospheric path. A simple correction was applied, mainly with the purpose of better identifying the same features at both PJ4 and PJ5. Since during PJ4 JIRAM observed the same regions of the north pole at different emission angles, those data were used to compile a look-up table that, given radiances measured at emission angles lower than 90°, permits scaling of the measured values to the radiances expected at 90° to make the measurements more comparable to each other.

Data are jovian-located and then re-projected in System III planetocentric geographical coordinates, using a polar orthographic projection. Geometric information was obtained by using *ad hoc* algorithms based on the NAIF-SPICE tool[24] for each image. JIRAM raw data are calibrated in units of radiance (W m^{-2} sr^{-1}) as described[16,17]. The responsivity used in this study has been revised to a flat value of 2×10^6 digital numbers (DN) per (W m^{-2} sr^{-1}) by using the cruise-calibration campaign data, performed by using the orange giant star Aldebaran (α Tauri) as a reference target.

Finally, the diameters of the cyclones are calculated on the JIRAM infrared images, defining the outer border of the cyclone where the smaller, anticyclonic structures form and planetocentric coordinates are used throughout this report. Images from JIRAM were processed using Matlab (Fig. 1 and Extended Data Fig. 1) and ENVI-IDL (Fig. 3).

Processing of consecutive images allows for animations revealing motion, as well as for quantitative analysis of cloud velocities. JIRAM data in Extended Data Table 1 have been arranged in animations that show the movement of single vortices during PJ4 observations. Each sequence or scan has been composed into a mosaic, and then each mosaic became a frame of the video. We provide nine Supplementary Videos for the north pole (eight for circumpolar cyclones plus the NPC); each video is made of 11 images. We also provide six Supplementary Videos for the south pole (five for circumpolar cyclones plus the SPC); each video is made of 6 images.

JunoCam. JunoCam is a visible-spectrum camera designed to acquire images through broadband red, green and blue filters mounted directly on a CCD detector, with an 889-nm methane absorption band filter acquiring an image on a separate rotation typically 30 s later. JunoCam is rigidly mounted on the spinning spacecraft. That way, it uses the spacecraft rotation to take a full panorama within about 30 s consisting of up to 82 narrow exposures, referred to as the 'pushframe' mode. Usually, it takes partial panoramas of the target of interest. The camera has a horizontal field of view of about 58°, and a Kodak KAI-2020 charge-coupled device (CCD) sensor with four filter stripes, a red, a green, a blue (RGB) and a narrow-band 890-nm infrared filter attached on the 1,600 × 1,200 light-sensitive pixels. For each of the four filters, there is an corresponding readout region of 1,600 × 128 pixels which can be transferred into the resulting raw image. This transfer is not immediate, but the 12-bit data number of each pixel is encoded as an 8-bit value, and tiles of 16 × 16 pixels are compressed in either a lossy or lossless manner. Usually, the encoding of the 12-bit data as an 8-bit value is nonlinear, according to a 'companding' function. Motion blur is mostly avoided by a technique called time delay integration. In colour (RGB) mode, for each exposure, three of the four readout regions are added as stripes to the raw image. Full details of the instrument and its operation are available in ref. 18.

JunoCam observed the same polar regions as JIRAM on PJ4 and PJ5—as well as complementary longitudinal regions on PJ1 and PJ3—but as a visible imager, it acquires images in reflected light. A complete polar view must be pieced together from the unshadowed portions of images collected during multiple perijove passes.

Observations were made in both north and south polar regions during PJ1, PJ3, PJ4 and PJ5. Polar imaging in PJ5 was scheduled over extended periods of time to cover more longitudes as the planet rotates through daylight, which enabled time-lapse measurments that include measurements of rotation of the cyclones.

With an approximate geometrical camera model, including its pointing for each exposure, the appropriate three-dimensional vector was calculated for each pixel in a given reference frame, for example, J2000. Position and pointing information are inferred from SPICE data[24], with some manual adjustment. Jupiter is modelled as a MacLaurin spheroid on Jupiter's 1-bar level. A planetocentric coordinate system assigns a three-dimensional position to each longitude/latitude pair. The three-dimensional vector, pointing from Juno to the three-dimensional position, completes the connection of each longitude/latitude pair to colour information. With this method, each raw JunoCam image of Jupiter is reduced to an approximately geometrically calibrated polar-map projection.

Because Jupiter is rotating and Juno is moving rapidly, the illumination for each JunoCam image changes rapidly. Comparison of images requires approximate normalization of the images. For now, this is achieved in a heuristic way, essentially stretching contrast over regions of approximately similar solar incidence angles, subtracting the mean brightness for these bins, and accounting for changing light scattering of a presumed haze layer as a function of emission angle, which can be obtained for sufficiently small crops by high-pass filtering. For the JunoCam maps shown in Figs 1 and 2, this correction was made down to a maximum solar illumination angle of 66°, above which the signal-to-noise ratio drops below a value of 3 per pixel. Further nonlinear brightness stretching and saturation enhancement brings out detail.

Time sequences of 2 to 3 frames of polar images were made on all perijove passes to track cloud motions. After PJ1, it was clear that the limited time sequence on that orbit verified the visible impression that the features surrounding the poles whose 'arms' implied cyclonic motion really were cyclones. A special effort was made in PJ5 to create longer sequences of time-lapse images that would illustrate subtler motions of the polar features by imaging over a longer time interval. The sequences given below represent three of the best of those animations. A sequence of images from the north pole is available at http://junocam.pictures/gerald/uploads/20170424/anim/jnc_pj05_N_089_to_105_blend4_enh.html. A sequence of images from the south pole is available at http://junocam.pictures/gerald/uploads/20170331/anim/jnc_pj05_polarS_60px_lin_interpolated_21frames_1200x1200.html. A close-up version of that south polar sequence is available at http://junocam.pictures/gerald/uploads/20170406/anim/jnc_pj05_south_polar_animation_111_to_121_8frames_20fps_1200px.html.

History and terminology of cyclone clusters. The term 'ditetragonal' has been introduced in the context of crystallography, since it is one of the ten two-dimensional crystallographic point groups (see table 10.1.2.1 in ref. 25). In the non-Euclidean geometry of the curved polar region, a two-dimensional pentagonal rather than a hexagonal pattern would be conceivable, similar to the surface of a pentagon-dodecahedron (see table 10.1.2.2 in ref. 25). But since the size of the vortices does not fit exactly to the geometry of a pentagon-dodecahedron, an unstable structure switching between a hexagon and pentagon could occur, or an oscillating pentagon for vortices of similar sizes. Besides the 'vortex crystals'[22,23] mentioned above, similar vortex patterns also occur in rotating superfluid helium II for quantum-mechanical reasons[26]. Theoretical predictions of such quantized vortices reach back to Onsager[27] and Feynman[28], although Landau[29] introduced rotons in 1941. The first experimental observations[30] were in 1979.

Data availability. The data used for this study will be available once the proprietary period ends, namely about six months after the data were collected by Juno, from the NASA's Planetary Data System at https://pds.jpl.nasa.gov/tools/data-search/. The JunoCam data are all available for direct download from the Mission Juno web site in both raw and processed form: https://www.missionjuno.swri.edu/junocam/processing.

24. Acton, C. H. Ancillary data services of NASA's navigation and ancillary information facility. *Planet. Space Sci.* **44,** 65–70 (1996).
25. Hahn, Th. (ed.) *International Tables for Crystallography* Vol. A, 5th edn, 768, 786 (Springer, 2005).
26. Aref, H. *et al.* Vortex crystals. *Adv. Appl. Mech.* **39,** 1–79 (2003).
27. Gorter, C. J. The two fluid model of helium II. *Nuovo Cimento* **6** (Suppl. 2), 245–250 (1949); see discussion by L. Onsager, 249–250.
28. Feynman, R. P. in *Progress in Low Temperature Physics* Vol. 1 (ed. Gorter, C. J.) Ch. II, 17–53 (Elsevier, 1955).
29. Landau, L. D. The theory of superfluidity of helium II. *Zh. Eksp. Teor. Fiz.* **11,** 592 (1941).
30. Yarmchuk, E. J., Gordon, M. J. V. & Packard, R. E. Observation of stationary vortex arrays in rotating superfluid helium. *Phys. Rev. Lett.* **43,** 214–217 (1979).

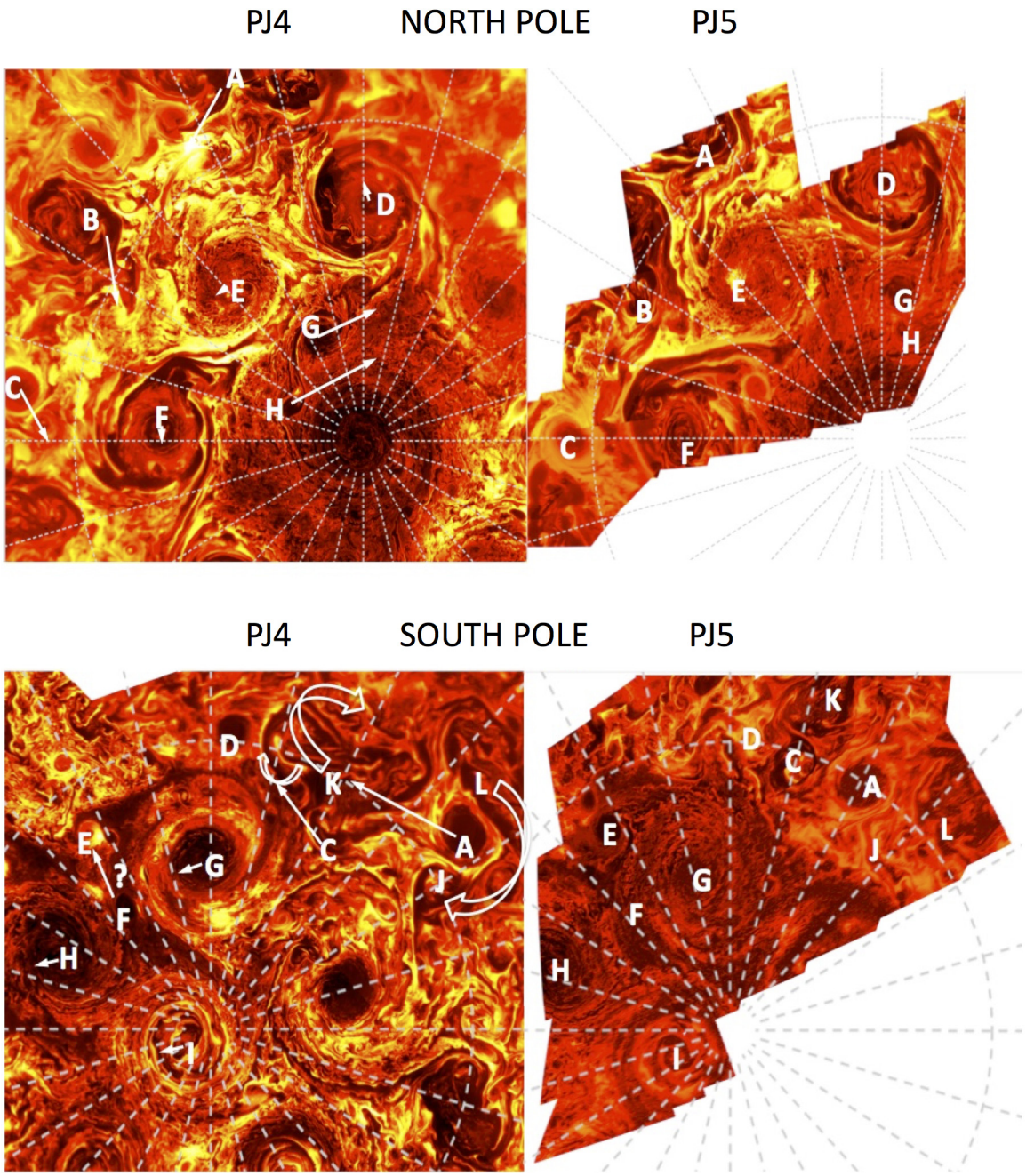

Extended Data Figure 1 | Comparison of the polar cyclonic structures between PJ4 and PJ5. Here is the comparison between JIRAM 5-μm data acquired during PJ4 and PJ5. The letters identify possible recurrent structures and arrows show the suggested displacements that occurred in the 53-day interval between these two perijoves. The radiance scale is the same as in Fig. 1. When the region surrounding the north pole is not sunlit, there are no JunoCam observations of the NPC. Although the north pole was detected by JIRAM on PJ4, we were unable to determine whether or not it maintains a stable position over the geographic north pole because of insufficient coverage of the NPC during PJ5. However, the cyclonic structures A, B and C move northeast, migrating from the lower latitudes. The G and H internal structures, located between the NPC and the cyclones, are anticyclones and move westward in that narrow corridor between 85.5° N and 87° N to their new location observed during PJ5 between vortex D and the NPC. In contrast, JIRAM was able to observe the SPC in both PJ4 and PJ5. In fact, along with the cyclones G and H shown, the SPC moves northward, increasing its distance with respect to the geographic south pole by 1.5° between PJ4 and PJ5. On the other hand, JunoCam was able to observe the SPC at all perijoves, and found that it was always displaced from the south pole in approximately the same direction (towards a System III longitude of about 219° ± 21°), with its central latitude varying from 88.0° S at PJ1 up to 89.0° S at PJ4, and down to 88.4° S at PJ5. It remains to be seen whether this is a cyclic oscillation. The five cyclones remain at almost constant radial distances from the centre of the SPC (and thus not from the geographic south pole), so the whole pentagon drifts in latitude. Anticyclone A appears to move as much as about 1° south and about 24° east. It is forced and surrounded by the two cyclonic structures that consolidate themselves between PJ4 and PJ5 from the origins L, J, C and K. Finally, the anticyclone D disappears while F is expelled from its position and possibly moves to new position E.

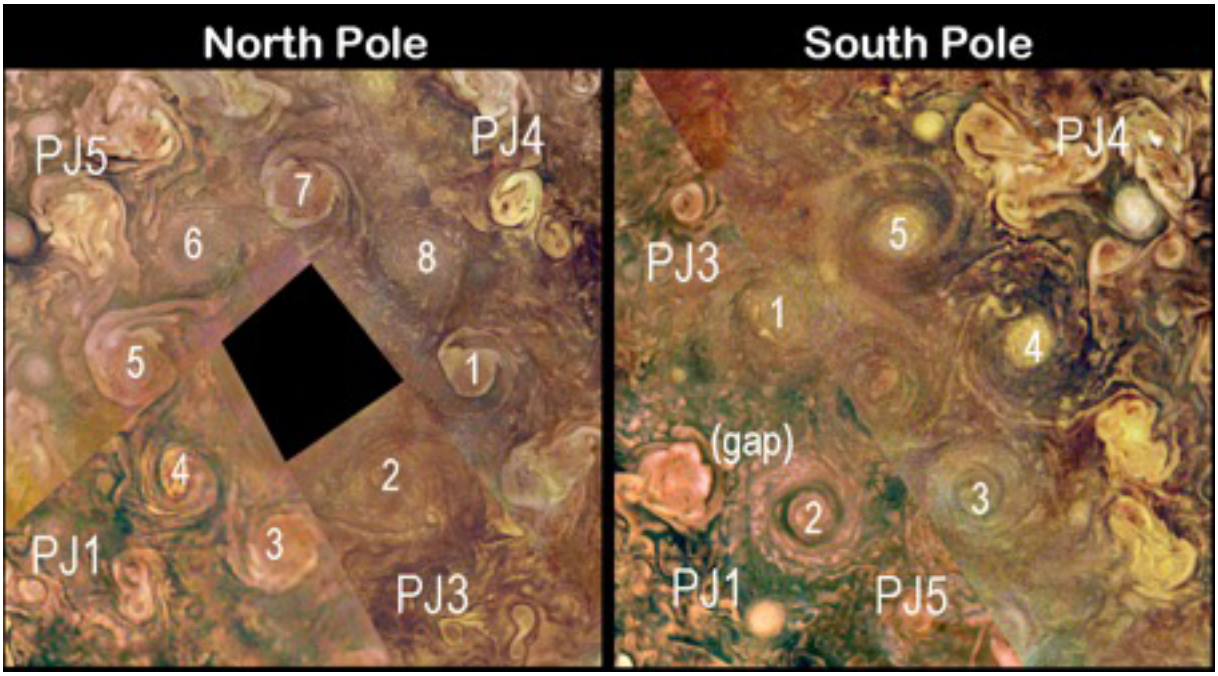

Extended Data Figure 2 | Annotated version of the JunoCam images of the poles. The unannotated version is shown in Fig. 2. The composite components from each perijove pass that were used to create the figure are noted. Each corresponds to the polar image taken at a time that minimized the emission angle over most of the pole, as detailed in Extended Data Table 2. The PJ4 component is identical to its contribution in Fig. 1, with contributions from the other perijove passes, separated by approximately 90° in longitude, as noted. The northern cyclones forming the inner square (actually a rhombus) of the ditetragonal pattern are labelled by odd numbers and those forming the outer square by even numbers. The southern cyclones forming a quasi-pentagonal shape are numbered sequentially, with the largest spacing between cyclones labelled 1 and 5, indicated by the 'gap' label. Despite the time differences of 53 to 106 terrestrial days between JIRAM images acquired on PJ4, shown broadly in Fig. 1b and d, and JunoCam images in PJ1, PJ3 and PJ5, the positions of the cyclones are remarkably consistent in System III longitude.

Extended Data Table 1 | JIRAM start time, stop time and number of observations for the different datasets used for this study

North Pole, 4th perijove, 2017-02-02		
Start UTC	Stop UTC	observations
08:10:24	08:15:59	12(1)
08:18:31	08:24:07	12(1)
08:26:08	08:31:44	12(1)
08:34:16	08:39:51	12(1)
08:42:23	08:47:59	12(1)
08:50:31	08:56:06	12(1)
08:58:08	09:03:43	12(1)
09:06:15	09:11:51	12(1)
09:14:23	09:19:58	12(1)
09:22:30	09:28:06	12(1)
09:30:07	09:35:43	12(1)
09:38:15	09:43:50	12(1)
09:46:22	09:51:58	12(1)
11:00:00	11:05:35	12(2)
11:08:07	11:13:43	12(2)
11:16:14	11:21:50	12(2)
11:24:22	11:29:57	12(2)
11:31:59	11:37:34	12(2)
11:40:06	11:45:41	12(2)
11:48:13	11:53:48	12(2)
11:56:20	12:01:55	12(2)
12:04:26	12:10:02	12(2)
12:12:02	12:17:38	12(2)
12:20:07	12:25:44	12(2)

South Pole, 4th perijove, 2017-02-02		
Start UTC	Stop UTC	observations
13:58:59	14:08:08	19
14:18:46	14:27:55	19
14:39:04	14:48:13	19
14:58:53	15:08:02	19
15:18:41	15:27:50	19
15:39:00	15:48:09	19

North Pole, 5th perijove, 2017-03-27		
Start UTC	Stop UTC	observations
08:14:20	08:16:20	5
08:18:49	08:24:19	12
08:26:48	08:30:48	9
08:33:17	08:33:47	2

South Pole, 5th perijove, 2017-03-27		
Start UTC	Stop UTC	observations
09:17:54	09:18:54	3
09:21:23	09:24:24	7
09:26:53	09:29:53	7
09:32:23	09:33:53	4

UTC, coordinated universal time. (1) Approach phase, low resolution; used only to fill small gaps in Fig. 1; (2) minimum emission angle, high resolution, used to make most of the mosaic in Fig. 1.

Extended Data Table 2 | Details of the JunoCam observations

Pole	Perijove	Date	Time (UTC)	File Name
North	1	2016-08-27	11:57:40-11:57:49	JNCE_2016240_00C06160_V02_553
South	1	2016-08-27	11:59:12-11:59:21	JNCE_2016240_00C06186_V02_579
North	3	2016-12-11	16:13:45-16:13:54	JNCE_2016346_03C00099_V02_588
South	3	2016-12-11	18:10:49-18:10:56	JNCE_2016346_03C00126_V02_615
North	4	2017-02-02	12:08:22-12:08:32	JNCE_2017033_04C00097_V01_624
South	4	2017-02-02	14:06:29-14:06:38	JNCE_2017033_04C00109_V01_636
North	5	2017-05-19	08:04:43-08:04:52	JNCE_2017086_05C00102_V01_890
South	5	2017-05-19	10:01:48-10:01:55	JNCE_2017086_05C00118_V01_901

The observations listed correspond to those used in Figs 1 and 2 and in Extended Data Fig. 2.